大阪公立大学
Osaka Metropolitan University
学術情報リポジトリ

Systematic Study of Descriptors for Oxygen Evolution Reaction Catalysis in Perovskite Oxides

メタデータ	言語: English 出版者: 公開日: 2019-01-31 キーワード (Ja): キーワード (En): 作成者: Yamada, Ikuya, Takamatsu, Akihiko, Asai, Kaisei, Shirakawa, Takuto, Ohzuku, Hideo, Seno, Akihiro, Uchimura, Tasuku, Fujii, Hiroshi, Kawaguchi, Shogo, Wada, Kouhei, Ikeno, Hidekazu, Yagi, Shunsuke メールアドレス: 所属:
URL	http://hdl.handle.net/10466/16192

Systematic Study of Descriptors for Oxygen Evolution Reaction Catalysis in Perovskite Oxides

Ikuya Yamada,[1,2] Akihiko Takamatsu,[2] Kaisei Asai,[1] Takuto Shirakawa,[1] Hideo Ohzuku,[2] Akihiro Seno,[2] Tasuku Uchimura,[1] Hiroshi Fujii,[2] Shogo Kawaguchi,[3] Kouhei Wada,[4] Hidekazu Ikeno,[1,2,5*] Shunsuke Yagi[6*]*

[1]Department of Materials Science, Graduate School of Engineering, Osaka Prefecture University, 1-2 Gakuen-cho, Naka-ku, Sakai, Osaka 599-8570, Japan

[2]NanoSquare Research Institute, Research Center for the 21st Century, Organization for Research Promotion, Osaka Prefecture University, 1-2 Gakuen-cho, Naka-ku, Sakai, Osaka 599-8570, Japan

[3]Japan Synchrotron Radiation Research Institute1-1 Kouto, Sayo-cho, Sayo-gun, Hyogo 679-5198, Japan

[4]Fuji Die Co., Ltd., 36-1 Hirasawa, Hadano, Kanagawa 257-0015, Japan

[5]Precursory Research for Embryonic Science and Technology (PRESTO), Japan Science and Technology Agency (JST), 4-1-8 Honcho Kawaguchi, Saitama 332-0012, Japan

[6]Institute of Industrial Science, University of Tokyo, 4-6-1 Komaba, Meguro-ku, Tokyo 153-8505, Japan

Abstract

Ever proposed descriptors of catalytic activity for oxygen evolution reaction (OER) were systematically investigated. A wide variety of stoichiometric perovskite oxides ABO_3 (A = Ca, Sr, Y, La; B = Ti, V, Cr, Mn, Fe, Co, Ni, Cu) were examined as OER catalysts. The simplest descriptor, e_g electron number of transition metal ion at B-site, was not applicable for OER overpotentials (η) of the compounds tested in this study. Another descriptor, oxygen 2p band center relative to Fermi energy (ε_{2p}), was not necessarily adequate for the most part of perovskite oxides. Eventually, a recently proposed descriptor, charge-transfer energy (Δ), displayed a linear relationship with η the most reasonably. Since Δ values were obtained from theoretical calculations, not only by spectroscopic experiments, systematic exploration for a wide range of compounds including hypothetical ones could be allowed. This finding proposes the charge-transfer energy as the most helpful descriptor for design of perovskite oxide catalyst for OER.

1. Introduction

The oxygen evolution reaction (OER, $4OH^- \rightarrow O_2 + 2H_2O + 4e^-$ in alkaline conditions) plays a crucial role in achieving renewable energy society because of the versatility for energy conversions such as water splitting and rechargeable metal-air batteries.[1-3] As well as precious-metal oxides,[4-6] perovskite oxides (ABO_3) consisting of earth-abundant transition metal elements have been extensively investigated as promising OER catalysts. Recent advances in experimental and computational techniques proposed rational descriptors for highly active OER catalysts beyond those reported several decades ago:[7, 8] metal-oxygen covalency,[9] metal-oxygen bond length/angle,[10-12] magnetic spin state,[13-15] oxygen diffusion rate,[16] e_g orbital occupancy,[17] oxygen 2p band center relative to Fermi level,[18] and charge-transfer energy.[19] Among them, the last three have attracted particular interest because of their simplicity. Suntivich et al.[17] proposed that the OER onset potentials for perovskite oxides follow a volcano-type plot, in which the lowest onset potential is achieved when the *B*-site transition metal ion has $e_g^{\sim 1.2}$ configuration for regular octahedral crystal field splitting. Grimaud et al.[18] demonstrated that OER onset potentials of Co-based perovskite oxides have a linear relationship with oxygen 2p band center energy level. Recently, Hong et al.[19] proposed that charge-transfer energy determined by X-ray spectroscopy experiments serves as an electronic descriptor to explain change in OER mechanism, followed by examination for selected perovskite oxides very recently.[12, 20]

Although the above descriptors are all focused on the metal-oxygen covalency to increase charge-transfer in rate-determining step of OER and applicable even for other systems,[21, 22] careful verification of universality and scope of application among a wide range of compounds is desired. Statistical analysis of a large number of data (101 observations of 51 compounds) proposed that a few electronic factors (d electron number, metal-oxygen covalency, and e_g occupancy) primarily

affect OER activity, in addition to significant structure effect of metal-oxygen bond angle.[23] Multiple descriptors are necessary to reasonably explain the OER activity and it is difficult to give a description with a sole descriptor.

Several active OER catalysts are reported for chemically complex perovskite oxides such as $Ba_{0.5}Sr_{0.5}Co_{0.8}Fe_{0.2}O_{3-\delta}$ (BSCF),[17] $LnBaCoO_{5+\delta'}$ (*Ln* = Pr, Sm, Gd, and Ho),[18] and $Sr(Co_{0.7}Fe_{0.2}Nb_{0.1})O_{3-\delta}$.[24] Despite of their high performance, precise theoretical study is generally difficult owing to their intrinsic randomness (oxygen deficiency, mixing of *A*/*B*-site atoms), thus acquisition of a simple descriptor based on theoretically proper electronic-state calculations from these catalysts are not able to be expected in this light.

We recently reported that perovskite oxides containing unusual high-valence Fe^{4+} ions, $CaFeO_3$ and $SrFeO_3$, exhibit OER catalytic activity comparable to BSCF.[25] Large differences in OER activity between nominally isoelectronic oxides with e_g^1 configuration, highly active (Ca/Sr)FeO_3 and poorly active $LaMnO_3$, could not be explained by the e_g occupancy descriptor.[17] Also, we reported the oxygen 2p band center descriptor is not realized in manganese perovskite oxides.[26] These counterexamples imply that it is desired to verify the adequacy of the ever proposed descriptors, but no careful examination was performed in a wide range of perovskite oxides. Systematic study on perovskite oxide catalysts containing various 3d transition metals (Ti, V, Cr, Mn, Fe, Co, Ni, and Cu) may clarify which factor is effective against OER catalytic activity beyond separate investigations exploring for highly active OER catalysis.

In this article, we demonstrate an experimental and theoretical study of OER catalysis for ABO_3-type perovskite oxides consisting of various 3d transition metal ions. We have found that the previously proposed descriptors, e_g electron number and oxygen 2p band center, are not necessarily applicable for a wide range of perovskite oxides. By contrast, we have found that charge-transfer

energy[19] obtained from density functional theory (DFT) calculation closely relates to the OER overpotential. This finding provides a rational design principle for OER catalysts based on pure electronic descriptor calculated theoretically.

2. Experimental and Computational Procedures

Sample Preparation

The perovskite oxides, Sr*B*O_3 (*B* = Ti, V, Cr, Mn, Fe, and Co), Y*B*O_3 (*B* = V, Cr, Mn, Fe, Co, and Ni), and La*B*O_3 (*B* = V, Cr, Mn, and Ni) were synthesized by solid-state reaction. Several compounds were synthesized under high pressures up to 12 GPa to stabilize perovskite structures ($SrVO_3$ and $SrCrO_3$)[27, 28] or fully oxidize in tetravalent states ($SrFeO_3$ and $SrCoO_3$).[29] $SrMnO_3$ with a cubic perovskite structure was obtained from hexagonal $SrMnO_3$ (4*H*-$SrMnO_3$) by annealing at 1773 K in an Ar flow and subsequently at 623 K in air.[30] All the data for Ca*B*O_3 (*B* = Ti, V, Cr, Mn, Fe, and Co), $LaFeO_3$, $LaCoO_3$, and $LaCuO_3$ were taken from the reference,[20] in which all the experiments and theoretical calculations were performed in the same manner as the present study. Six reference samples of solid solutions with nominal half-integer e_g electron configurations, $Sr_{0.5}La_{0.5}MnO_3$, $CaMn_{0.5}Fe_{0.5}O_3$, and $SrMn_{0.5}Fe_{0.5}O_3$ for $e_g^{0.5}$, $Ca_{0.5}La_{0.5}FeO_3$, $Sr_{0.5}La_{0.5}FeO_3$, and $LaMn_{0.5}Fe_{0.5}O_3$ for $e_g^{1.5}$, were also prepared at ambient- and high-pressure conditions. The detail synthesis conditions are listed in Table S1 in the Supporting Information.

Basic Characterization

X-ray powder diffraction (XRD) patterns were collected by using X-ray diffractometer with Cu Kα radiation (Ultima IV, Rigaku, Japan). Synchrotron X-ray powder diffraction (SXRD) patterns at room temperature were collected using a Debye-Scherrer camera installed at the BL02B2 beamline of SPring-8, Japan.[31] The wavelength was determined to approximately 0.5 Å using

CeO_2 as reference. The SXRD data were analyzed using Rietveld refinement program RIETAN-FP.[32] Specific surface area was estimated by the Brunauer-Emmett-Teller analysis of Kr gas adsorption data (BELSORP-max, MicrotracBEL, Japan).

Electrochemical Characterization

OER catalytic activities were evaluated by using rotating disk electrode system in the same manner as the previous study.[20, 25, 26] A 5 wt% proton-type Nafion suspension (Sigma-Aldrich), 0.1 M KOH aqueous solution (Nacalai Tesque, Inc., Japan), and tetrahydrofuran (THF, Sigma-Aldrich) were mixed in a 2:1:97 volume ratio. The catalyst ink was prepared by mixing 5 mg of catalyst, 1 mg of acetylene black (Denka Co., Ltd., Japan), and 1mL of the above THF solution. A 6.4 μL of catalyst ink was taken with stirring and drop cast onto the glassy-carbon disk electrode (4 mm in diameter). Electrochemical measurements were performed using a rotating-disk electrode rotator (RRDE-3 A, BAS Inc., Japan) in combination with a bipotentiostat (Model-2325, BAS Inc., Japan). Pt wire and Hg/HgO electrodes (International Chemistry Co., Ltd., Japan) filled with a 0.1 M KOH aqueous solution (Nacalai Tesque, Inc., Japan) were used as the counter and reference electrodes, respectively. All electrochemical measurements were conducted under O_2 saturation at room temperature. This fixed the equilibrium potential of the O_2/H_2O redox couple to 0.304 V versus Hg/HgO. The disk potential was controlled between 0.3 and 0.9 V versus Hg/HgO at a scan rate of 10 mV s^{-1} and disk rotation rate was set at 1600 rpm. The disk potentials are represented in those versus reversible hydrogen electrode (RHE), together with *iR*-compensation (R ~43 Ω). The capacitive effect was compensated by averaging the cathodic and anodic scans.

DFT calculation

Spin-polarized DFT calculations were systematically performed for perovskite oxides, namely, SrBO$_3$ (B = Ti, V, Cr, Mn, Fe, and Co), YBO$_3$ (B = V, Cr, Mn, Fe, Co, and Ni), and LaBO$_3$ (B = V, Cr, Mn, Co, Ni, and Cu). The calculations were made using the plane-wave based projector augmented wave (PAW) method as implemented in the Vienna *Ab-initio* Simulation Package (VASP).[33-35] The wavefuncitons were expanded in a plane-wave basis set with an energy cutoff of 500 eV. The exchange-correlation interactions were treated within the generalized gradient approximation (GGA) using the Perdew-Burke-Ernzerhof (PBE) functional. The strong on-site Coulombic interactions on the localized 3d electrons were treated with the GGA+U approach,[36] in which the U_{eff} parameters were chosen to reproduce the experimental oxidation enthalpy, as reported previously.[37, 38] Radial cutoff and valence electrons for PAW potentials, as well as U_{eff} parameters for 3d electrons adopted in this work are summarized in Table S2. The magnetic structures and nominal electron configurations considered in this work are summarized in Table S3. For k-point sampling, the mesh $k_1 \times k_2 \times k_3$ was prepared in accordance with the Monkhorst-Pack scheme, where the mesh count in each direction was selected as the near natural number of 40 per lattice parameter (1 Å^{-1}). The lattice constants and internal coordinates were optimized until the total energy difference and residual forces converged to less than 10^{-5} and 10^{-2} eV Å^{-1}.

The oxygen 2p band centers and unoccupied 3d band centers of transition metal atoms were computed from the projected density of states (DOS).[20] Oxygen 2p band center (ε_{2p})[18] was obtained by eq. 1 as:

$$\varepsilon_{2p} = \frac{\int_{-\infty}^{E_F} E f_{2p}(E) dE}{\int_{-\infty}^{E_F} f_{2p}(E) dE} \quad (1)$$

where $f_{2p}(E)$ is DOS projected on 2p orbitals of oxygen and E_F is the Fermi energy. Transition metal unoccupied 3d band center ($\varepsilon_{3d\text{-}un}$) was calculated by eq. 2 as:

$$\varepsilon_{3d-un} = \frac{\int_{E_F}^{E_{\max}} E f_{3d}(E) dE}{\int_{E_F}^{E_{\max}} f_{3d}(E) dE} \quad (2)$$

where $f_{3d}(E)$ is DOS projected on 3d orbitals of the transition metal, and $E_{\max}$ is the upper bound of unoccupied 3d bands. The value of $E_{\max}$ was selected so as to discard the insignificant peaks (smaller than 0.1) at higher energy of 3d projected DOS. The number of conduction bands were increased until the shapes of projected DOS were converged. Band centers and charge-transfer energies are summarized in Table S3.

3. Results and Discussion

Perovskite oxides consisting of a single 3d transition metal element from Ti to Cu were synthesized by solid-state reactions under ambient- and high-pressure (~8 GPa) conditions. High-pressure synthesis with strong oxidizing agent ($KClO_4$) enables entire filling of oxygen atoms even for late 3d transition metal oxides with high valences (e.g. $SrFe^{4+}O_3$, $SrCo^{4+}O_3$, and $LaNi^{3+}O_3$). XRD patterns in Figure 1 display that perovskite oxides were obtained in almost single phase. The lattice constants obtained from Rietveld refinement (Table S4) were close to the values reported previously. Specific surface areas ranged from 0.34–2.9 m^2/g (see Table S4), which are typical values for metal oxides synthesized by high-temperature solid-state reactions.

Figure 2 displays linear sweep voltammograms in OER conditions for 25 kinds of perovskite oxide catalysts: Ca*B*O_3 (*B* = Ti, V, Cr, Mn, Fe, Co; data taken from reference[20]), Sr*B*O_3 (*B* = Ti, V, Cr, Mn, Fe, Co), Y*B*O_3 (*B* = V, Cr, Mn, Fe, Co, Ni), and La*B*O_3 (*B* = V, Cr, Mn, Fe, Co, Ni, Cu; data for Fe, Co, and Cu taken from reference[20]). The OER onset potentials (E_{onset}) were determined as the potential in which the current densities per catalyst surface areas exceeded 0.05 mA cm^{-2}_{oxide}, in accordance with the previous studies,[17, 20, 25] and the OER overpotentials (η) were calculated by subtracting the theoretical OER potential (1.23 V vs. RHE): $\eta = E_{\text{onset}} - 1.23$ V. The

left panels in Figure 2 roughly represented that late 3d elements (Mn/Fe–Cu) were superior to early ones (Ti–Cr/Mn) for any perovskite series. Overpotentials for several compounds could not available because of their poor activities not attaining the threshold value (see right panels in Figure 2). These compounds were excluded from analyses of OER overpotential and descriptor hereinafter. Figure 3a illustrates the dependence of η values on *B*-site element (also see the numerical η values in Table S5). The η values roughly decreased from early (Ti–Cr/Mn) to late (Mn/Fe–Cu) elements. Increase in transition metal valence from trivalent (B^{3+} for $A = Y^{3+}$, La^{3+}) to tetravalent (B^{4+} for $A = Ca^{2+}$, Sr^{2+}) efficiently lowered η by ~0.05–0.1 V in most cases. Comparison of specific activities (current densities at 1.6 V vs. RHE) is illustrated in Figure 3b. Oxides with higher valences and late 3d transition metal elements tend to exhibit higher specific activities. On the above examination, the OER catalysis is maximized for $B = Fe^{4+}$ and Co^{4+}. Therefore, Fe^{4+}/Co^{4+}-containing perovskite oxides, $CaFeO_3$, $SrFeO_3$, and $SrCoO_3$, are the best OER catalysts for pure perovskite oxides. Tafel plots also demonstrated similar tendency (Figure S1 and Table S5 in the Supporting Information), in which Fe^{4+}-oxides had the smallest Tafel slope values. The difference in overpotential and specific activity between isoelectronic compounds variously changed. For example, the difference in overpotential ($\Delta\eta = 0.18$ V) between $CaMnO_3$ and $SrMnO_3$ was significant whereas very slight ($\Delta\eta = 0.01$ V) between $CaFeO_3$ and $SrFeO_3$. This is also a point to intrigue structure-activity relationship within isoelectronic compounds. However, we do not intend to study investigate individual cases in this study.

Previously proposed descriptors for OER catalysis were examined based on the above-demonstrated experimental data. A volcano-type plot along the e_g electron number was originally proposed by Suntivich et al.,[17] and is widely accepted at present.[21, 22, 39-48] Figure 4a shows η versus e_g electron number for the perovskite oxides, where the e_g electron numbers were estimated from

the most likely electron configurations (Table S3). Less active compounds ($CaTiO_3$, $CaCrO_3$, $SrTiO_3$, $SrVO_3$, YVO_3, $YCrO_3$, $LaVO_3$, and $LaCrO_3$) were excluded in this plot because the η values could not be defined. The η values widely ranged in any electron configurations: 0.36–0.54 V for e_g^0, 0.33–0.56 V for e_g^1, and 0.40–0.50 V for e_g^2. The average η values at each configuration were calculated to be 0.47(±0.08), 0.40(±0.08), and 0.44(±0.06) V for e_g^0, e_g^1, and e_g^2, respectively. Indeed, these average values apparently followed a gradient volcano-like shape (dashed curve in Figure 4a). However, compared with the previous report,[17] it does not efficiently serve to describe OER activity because of wide dispersion of data points (see error bars in Figure 4a). To compensate the data of non-integer e_g configurations, we also studied the solid solutions between compounds at e_g^0, e_g^1, and e_g^2 configurations (see Figure S2 in the Supporting Information). The nominal $e_g^{0.5}$ and $e_g^{1.5}$ configurations were obtained by chemical substitution of either *A*- or *B*-site, forming three solid solution series from e_g^0 to e_g^1 to e_g^2, as shown in Figure 4b. Two series, $SrMnO_3$ (e_g^0) – $SrMn_{0.5}Fe_{0.5}O_3$ ($e_g^{0.5}$) – $SrFeO_3$ (e_g^1) – $Sr_{0.5}La_{0.5}FeO_3$ ($e_g^{1.5}$) – $LaFeO_3$ (e_g^2) and $CaMnO_3$ (e_g^0) – $CaMn_{0.5}Fe_{0.5}O_3$ ($e_g^{0.5}$) – $CaFeO_3$ (e_g^1) – $Ca_{0.5}La_{0.5}FeO_3$ ($e_g^{1.5}$) – $LaFeO_3$ (e_g^2), roughly depicted volcano-type plots. In contrast, the other system, $SrMnO_3$ (e_g^0) – $Sr_{0.5}La_{0.5}MnO_3$ ($e_g^{0.5}$) – $LaMnO_3$ (e_g^1) – $LaMn_{0.5}Fe_{0.5}O_3$ ($e_g^{1.5}$) – $LaFeO_3$ (e_g^2), represented a reverse volcano shape. This contradiction indicates a clear counterexample to the proposed volcano-type plot. Therefore, we conclude that the e_g electron number can be utilized for selected compounds but is not a universal descriptor any more.

Trends in electronic states were investigated by DFT calculations. The *B*-site element dependence of oxygen 2p band center energies (ε_{2p}) are shown in Figure 5a. The ε_{2p} values for tetravalent oxides ($CaBO_3$ and $SrBO_3$) were slightly closer to Fermi level (0 eV) than trivalent oxides (YBO_3 and $LaBO_3$). This implies superiority for the former in the identical elements

according to the previous report.[18] Figure 5b illustrates unoccupied 3d band centers ($\varepsilon_{3d\text{-}un}$) for the perovskite oxides. The $\varepsilon_{3d\text{-}un}$ values for trivalent transition metal oxides with identical *B*-site elements (e.g. $YMn^{3+}O_3$ and $LaMn^{3+}O_3$) were almost the same, whereas those for tetravalent metal oxides exhibited relatively large differences (~1 eV). Theoretical charge-transfer energies (Δ) were calculated by the difference between $\varepsilon_{3d\text{-}un}$ and ε_{2p}: $\Delta = \varepsilon_{3d\text{-}un} - \varepsilon_{2p}$ (Figure 5c). It is obvious that the Δ values with identical ions are almost the same and systematically decreased from Ti to Cu, in stark contrast to unsystematic trend in ε_{2p} and $\varepsilon_{3d\text{-}un}$. The Δ values decreased by ~1 eV from trivalent to tetravalent state for each transition element.

Hereafter, we examine DFT-based descriptors for OER overpotentials and specific activities. Figure 6a shows the η as a functions ε_{2p}. The 17 data points disperse widely, inconsistent with the previous report, in which all the data points follow a linear relationship without large deviation, except for a few amorphized compounds.[18] Since the coefficient of determination (R^2) obtained by a linear fitting ($R^2 = 0.268$) was far from the unity, thus this descriptor is not utilized for a wide range of compounds. Charge-transfer energy (Δ) was recently proposed as a descriptor to represent specific activities.[19] The Δ values can be obtained by both experiments[19] and DFT calculations.[12] We have recently reported that $CaBO_3$ series and several perovskite oxides roughly follow a linear relationship between η and Δ, as well as quadruple perovskite oxides.[20] We examine unoccupied 3d band centers ($\varepsilon_{3d\text{-}un}$) in addition to Δ. Figure 6b demonstrates η versus $\varepsilon_{3d\text{-}un}$. The η versus $\varepsilon_{3d\text{-}un}$ plot roughly follows a linear dependence, obtained a much better R^2 value ($R^2 = 0.617$) than the η–ε_{2p} plot. This is the first indication that the unoccupied 3d bands are closely related to the OER activity. The role of unoccupied 3d band has not been attentively considered, but the present study proposes the importance of this band in OER. The η as a function of Δ is displayed in Figure 6c. The data points followed a line more closely and the correlation is increased ($R^2 = 0.686$). Note

that this relationship includes a wide range of perovskite catalysts with overpotentials from lower (~0.3 V) to higher (~0.55 V).

Specific activity is another index[19] thus examined by using the above DFT-based descriptors. Figure 6d represents a correlation between specific activity at 1.6 V vs. RHE and ε_{2p}, in which all the tested compounds (25 data points) are included. There was no clear relationship, supported by a very small coefficient of determination ($R^2 = 0.081$) as well as the η–ε_{2p} plot. Figure 6e displays correlation with unoccupied 3d band center, exhibiting a better linear relationship ($R^2 = 0.593$). A rational correlation with charge-transfer energy ($R^2 = 0.610$) was also observed (Figure 6f). These results indicate that charge-transfer energy is the most useful descriptor, leading to a model of the charge-transfer energies between adsorbates and transition metals (denoted as Δ' in Figure 7), in which O 2p band centers of adsorbates are linked to those in bulk. Δ' is related to the energy barrier in the charge-transfer process at the rate-determining step of OER. As Δ decreases, Δ' may also decrease and lower this energy barrier, which enhances the OER catalytic activities. The present study also confirms that a single descriptor does not necessarily explain OER catalysis. Thus, further studies based on informatics methodology are needed to elucidate the relationship between electronic states and OER catalytic activity.

4. Conclusions

We systematically investigated OER catalysis for ABO_3-type perovskite oxides and examined adequacy of descriptors ever proposed. The e_g electron number of transition metal ion and oxygen 2p band center were not applicable to wide range of compounds. In contrast, the charge-transfer energy obtained from DFT calculations was the most appropriate descriptor, suggesting a simple model that charge-transfer energies in bulk are associated with those between transition metal and adsorbate.

ASSOCIATED CONTENT

Supporting Information.

Synthesis conditions, computational conditions, all relevant experimental data, DFT calculation data, and linear sweep voltammograms of solid solution samples (PDF)

AUTHOR INFROMATION

Corresponding Authors

*yamamda@mtr.osakafu-u.ac.jp (I.Y.)

*ikeno@mtr.osakafu-u.ac.jp (H.I.)

*syagi@iis.u-tokyo.ac.jp (S.Y.)

Notes

The authors declare no competing financial interest.

ACKNOWLEDGMENTS

The authors thank Dr. Naoto Umezawa and Dr. Hideki Abe for fruitful discussion. The synchrotron radiation experiments were performed at SPring-8 under the approval of the Japan Synchrotron Radiation Research Institute (Proposal Numbers 2017B1077, 2017B1900, and 2018A1077). This work was supported by JSPS KAKENHI (Grant Numbers JP15H04169, JP16H04220, JP16H00893, JP17K18973, JP17K19182, JP18H03835), Murata Science Foundation, and Toray Science Foundation.

Figure Caption

Figure 1. XRD patterns of (a) SrBO$_3$ (B = Ti, V, Cr, Mn, Fe, Co), (b) YBO$_3$ (B = V, Cr, Mn, Fe, Co, Ni), and (c) LaBO$_3$ (B = V, Cr, Mn, Fe, Co, Ni, Cu).

Figure 2. Linear sweep voltammograms of (a) CaBO$_3$ (B = Ti, V, Cr, Mn, Fe, Co), (b) SrBO$_3$ (B = Ti, V, Cr, Mn, Fe, Co), (c) YBO$_3$ (B = V, Cr, Mn, Fe, Co, Ni), and (d) LaBO$_3$ (B = V, Cr, Mn, Fe, Co, Ni, Cu). The yellow lines represent current densities of 0.05 mA cm$^{-2}_{\text{oxide}}$, which determine onset OER potentials. The upper and bottom panels display entire and enlarged ranges, respectively.

Figure 3. OER overpotentials and specific activities for perovskite oxides.

Figure 4. OER overpotentials (η) versus e_g electron number. (a) Pure perovskite oxides: CaBO$_3$ (B = V, Mn, Fe, and Co; black squares), SrBO$_3$ (B = Cr, Mn, Fe, and Co; red circles), YBO$_3$ (B = Mn, Fe, Co, and Ni; green triangles), and LaBO$_3$ (B = Mn, Fe, Co, Ni, and Cu; blue reverse triangles). The gray diamonds and dashed line represent average η values at e_g^0, e_g^1, and e_g^2 configurations. The error bars illustrate standard deviations. (b) Solid solutions: SrMn$_{1-x}$Fe$_x$O$_3$ and Sr$_{1-x}$La$_x$FeO$_3$ (blue triangles), CaMn$_{1-x}$Fe$_x$O$_3$ and Ca$_{1-x}$La$_x$FeO$_3$ (green circles), Sr$_{1-x}$La$_x$MnO$_3$ and LaMn$_{1-x}$Fe$_x$O$_3$ (red squares). Gray open circles represent the data in the reference.[17]

Figure 5. Band centers and charge-transfer energy for perovskite oxides obtained from DFT calculations: (a) O 2p band center (ε_{2p}), (b) unoccupied 3d band center ($\varepsilon_{3d\text{-}un}$), and (c) charge-transfer energy (Δ).

Figure 6. OER overpotential (η) versus (a) O 2p band center (ε_{2p}), (b) unoccupied 3d band center ($\varepsilon_{3d\text{-}un}$), and (c) charge-transfer energy (Δ), and specific activity versus (d) ε_{2p}, (e) $\varepsilon_{3d\text{-}un}$, and (f) Δ. The purple lines were obtained from fitting.

Figure 7. Schematics of charge-transfer energies in bulk (Δ) and those between catalyst metals and adsorbates (Δ').

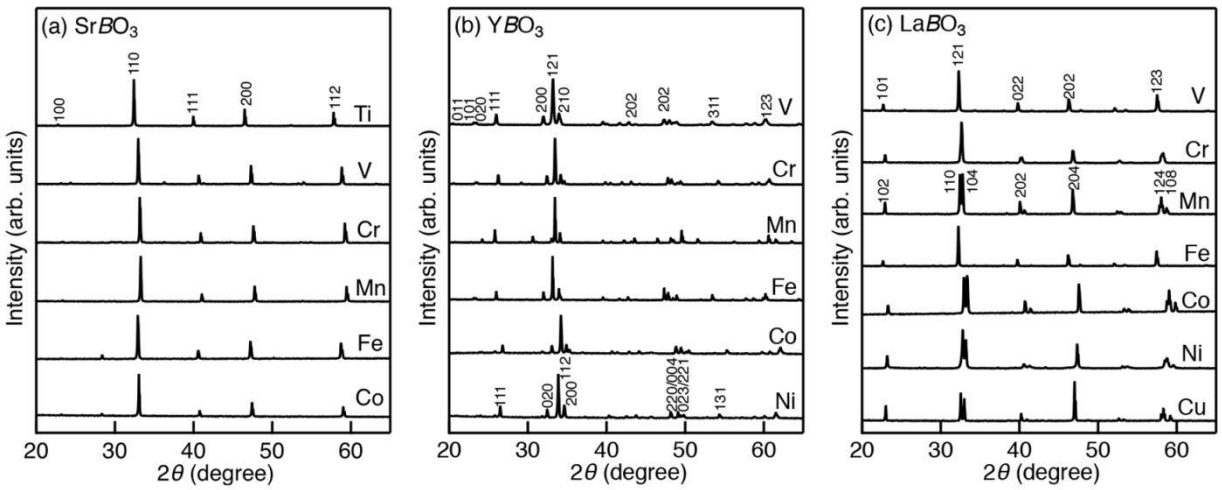
(a) SrBO3
(b) YBO3
(c) LaBO3
Intensity (arb. units)
2θ (degree)
Ti
V
Cr
Mn
Fe
Co
Ni
Cu

Figure 1

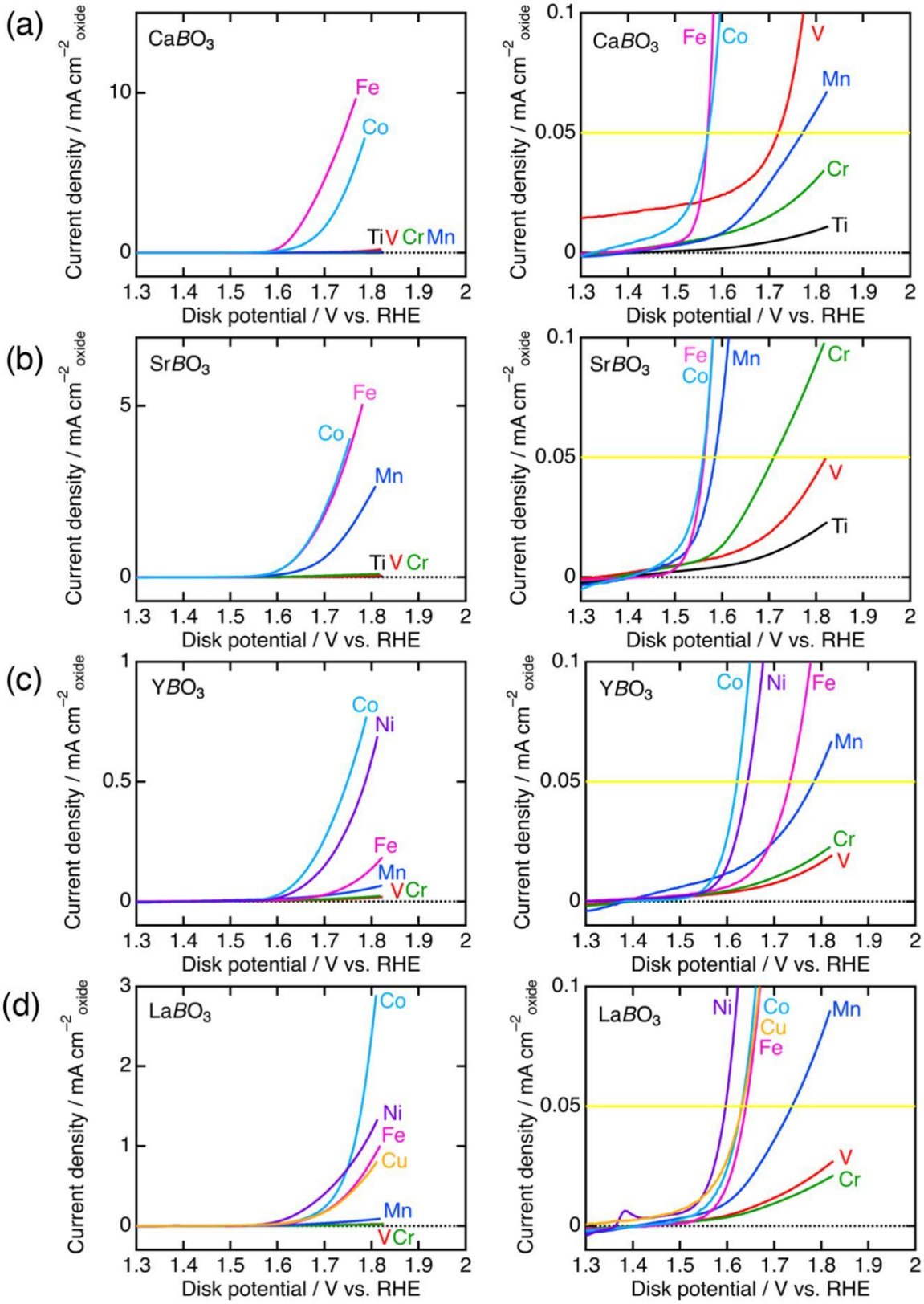
(a)
CaBO3
Fe
Co
Ti V Cr Mn
Mn
Cr
Ti
(b)
SrBO3
Fe
Co
Mn
Ti V Cr
V
Ti
(c)
YBO3
Co
Ni
Fe
Mn
V Cr
Cr
V
(d)
LaBO3
Co
Ni
Fe
Cu
Mn
V Cr
Cu
Current density / mA cm−2 oxide
Disk potential / V vs. RHE

Figure 2

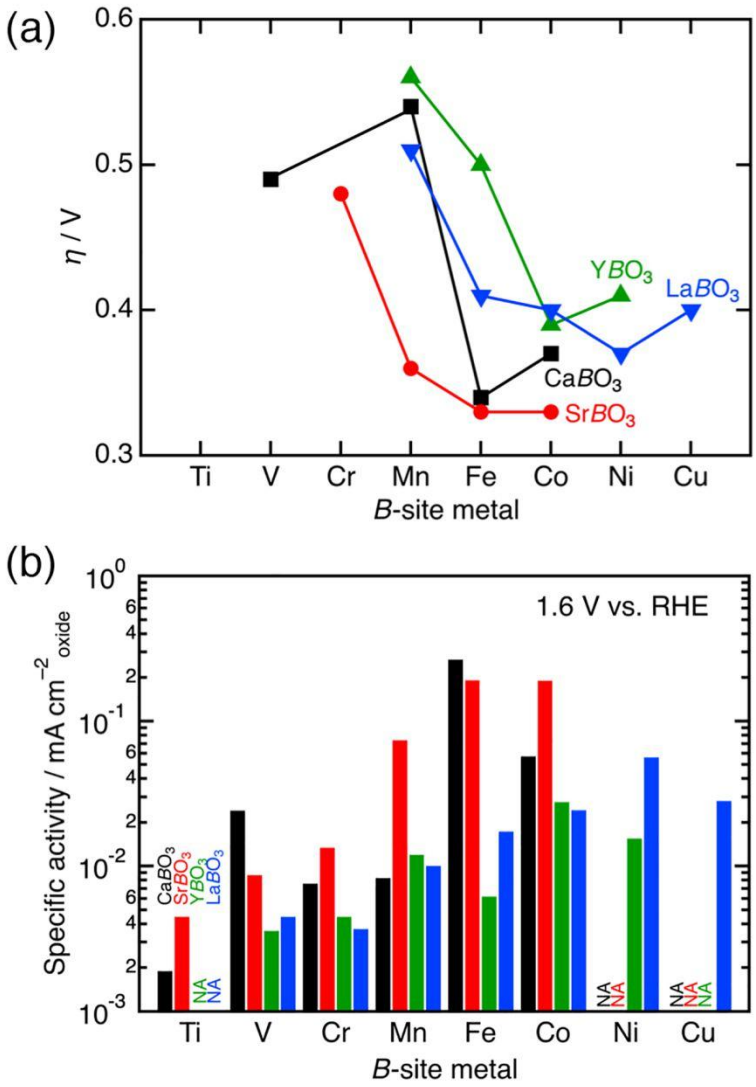
(a)
0.6
0.5
0.4
0.3
η / V
YBO3
LaBO3
CaBO3
SrBO3
Ti
V
Cr
Mn
Fe
Co
Ni
Cu
B-site metal
(b)
1.6 V vs. RHE
Specific activity / mA cm-2 oxide
10^0
10^-1
10^-2
10^-3
CaBO3
SrBO3
YBO3
LaBO3
NA
B-site metal

Figure 3

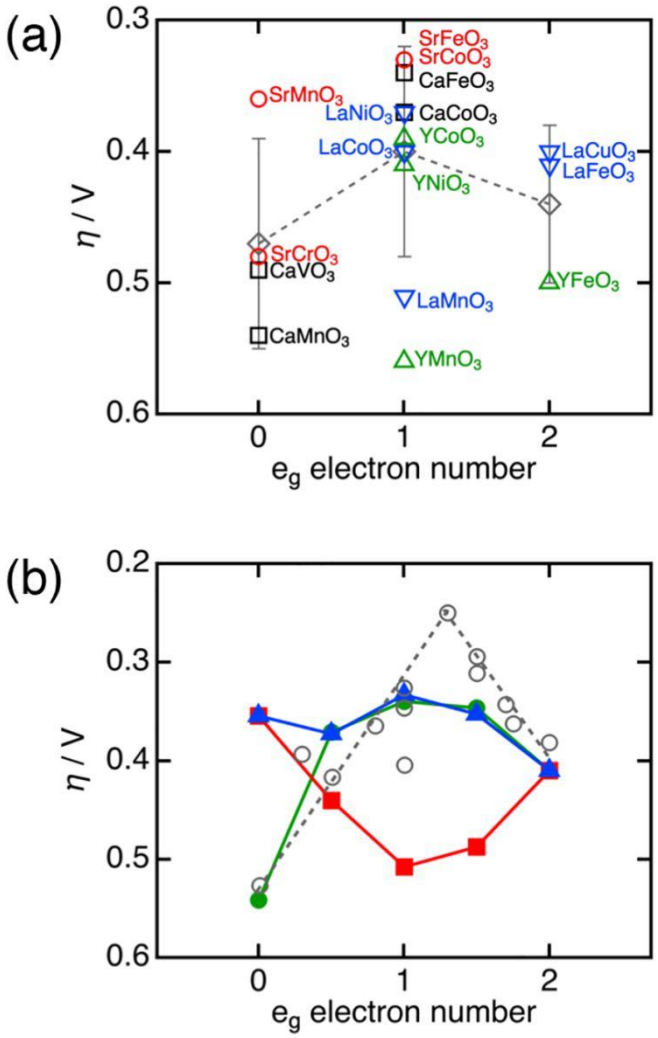
(a)
0.3
0.4
0.5
0.6
η / V
0
1
2
e_g electron number
SrFeO3
SrCoO3
CaFeO3
SrMnO3
LaNiO3
CaCoO3
YCoO3
LaCoO3
LaCuO3
LaFeO3
YNiO3
SrCrO3
CaVO3
YFeO3
LaMnO3
CaMnO3
YMnO3
(b)
0.2
0.3
0.4
0.5
0.6
η / V
0
1
2
e_g electron number

Figure 4

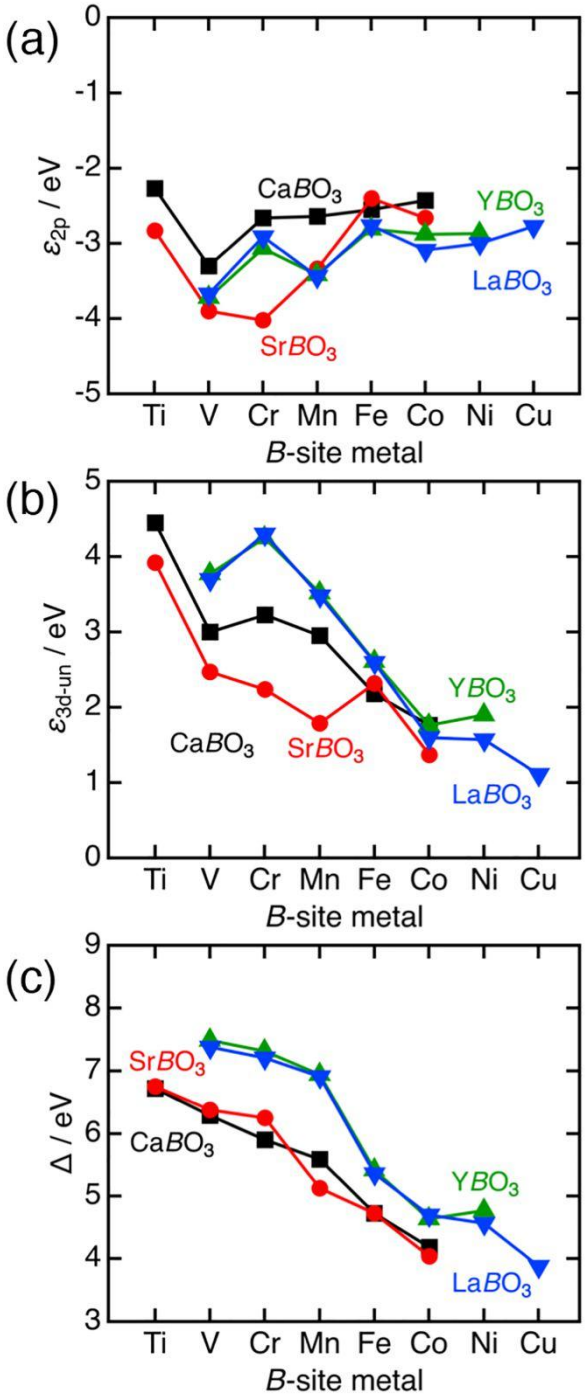
(a)
ε_{2p} / eV
0
-1
-2
-3
-4
-5
$CaBO_3$
YBO_3
$LaBO_3$
$SrBO_3$
Ti V Cr Mn Fe Co Ni Cu
B-site metal
(b)
$\varepsilon_{3d\text{-}un}$ / eV
5
4
3
2
1
0
YBO_3
$CaBO_3$
$SrBO_3$
$LaBO_3$
Ti V Cr Mn Fe Co Ni Cu
B-site metal
(c)
Δ / eV
9
8
7
6
5
4
3
$SrBO_3$
$CaBO_3$
YBO_3
$LaBO_3$
Ti V Cr Mn Fe Co Ni Cu
B-site metal

Figure 5

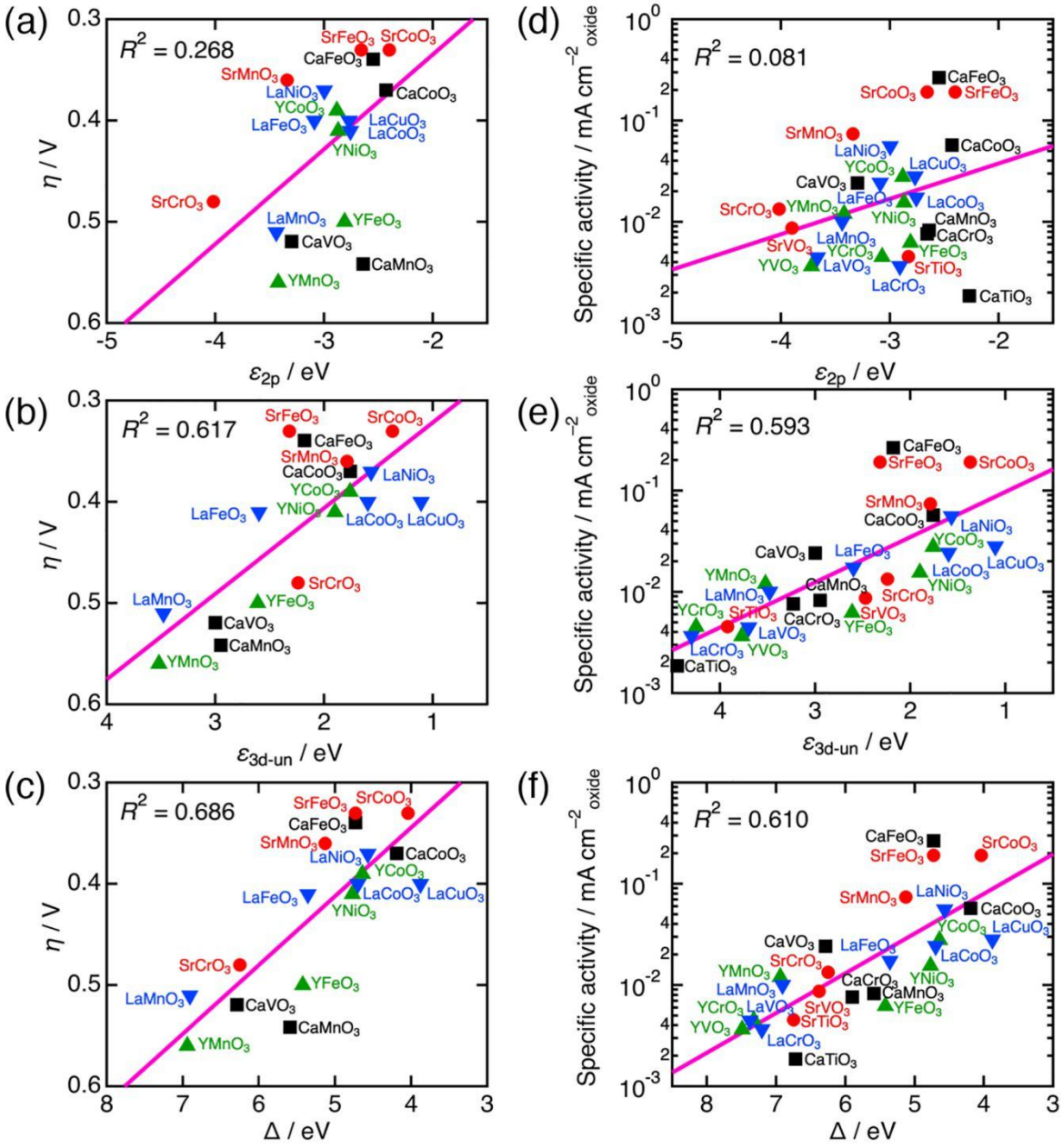
(a)
R^2 = 0.268
η / V
ε_{2p} / eV
(b)
R^2 = 0.617
η / V
$\varepsilon_{3d\text{-}un}$ / eV
(c)
R^2 = 0.686
η / V
Δ / eV
(d)
R^2 = 0.081
Specific activity / mA cm$^{-2}_{oxide}$
ε_{2p} / eV
(e)
R^2 = 0.593
Specific activity / mA cm$^{-2}_{oxide}$
$\varepsilon_{3d\text{-}un}$ / eV
(f)
R^2 = 0.610
Specific activity / mA cm$^{-2}_{oxide}$
Δ / eV
SrFeO3
SrCoO3
CaFeO3
SrMnO3
LaNiO3
CaCoO3
YCoO3
LaFeO3
LaCuO3
LaCoO3
YNiO3
SrCrO3
LaMnO3
YFeO3
CaVO3
CaMnO3
YMnO3
CaCrO3
SrVO3
YCrO3
YVO3
LaVO3
SrTiO3
LaCrO3
CaTiO3

Figure 6

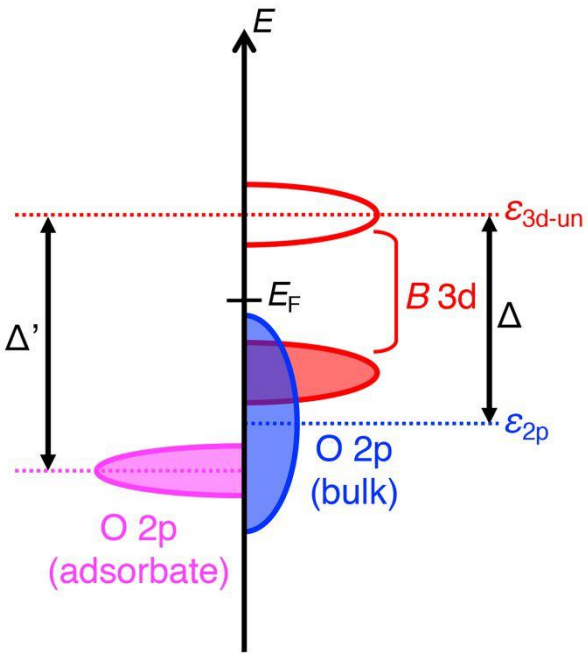
E
$\varepsilon_{3d\text{-}un}$
E_F
B 3d
Δ
Δ'
ε_{2p}
O 2p
(bulk)
O 2p
(adsorbate)

Figure 7

REFERENCES

(1) Cheng, Y.; Jiang, S. P. Advances in electrocatalysts for oxygen evolution reaction of water electrolysis-from metal oxides to carbon nanotubes. *Progress in Natural Science: Materials International* **2015,** *25*, 545-553.

(2) Fabbri, E.; Habereder, A.; Waltar, K.; Kötz, R.; Schmidt, T. J. Developments and perspectives of oxide-based catalysts for the oxygen evolution reaction. *Catal. Sci. Technol.* **2014,** *4*, 3800-3821.

(3) Hong, W. T.; Risch, M.; Stoerzinger, K. A.; Grimaud, A.; Suntivich, J.; Shao-Horn, Y. Toward the rational design of non-precious transition metal oxides for oxygen electrocatalysis. *Energy Environ. Sci.* **2015,** *8*, 1404-1427.

(4) Bloor, L. G.; Molina, P. I.; Symes, M. D.; Cronin, L. Low pH electrolytic water splitting using earth-abundant metastable catalysts that self-assemble in situ. *J. Am. Chem. Soc.* **2014,** *136*, 3304-3311.

(5) Stoerzinger, K. A.; Qiao, L.; Biegalski, M. D.; Shao-Horn, Y. Orientation-dependent oxygen evolution activities of rutile IrO_2 and RuO_2. *J. Phys. Chem. Lett.* **2014,** *5*, 1636-1641.

(6) Lee, Y.; Suntivich, J.; May, K. J.; Perry, E. E.; Shao-Horn, Y. Synthesis and activities of rutile IrO_2 and RuO_2 nanoparticles for oxygen evolution in acid and alkaline solutions. *J. Phys. Chem. Lett.* **2012**, *3*, 399-404.

(7) Bockris, J. O. M.; Otagawa, T. The electrocatalysis of oxygen evolution on perovskites. *J. Electrochem. Soc.* **1984,** *131*, 290-302.

(8) Bockris, J. O.; Otagawa, T. Mechanism of oxygen evolution on perovskites. *J. Phys. Chem.* **1983,** *87*, 2960-2971.

(9) Suntivich, J.; Hong, W. T.; Lee, Y.-L.; Rondinelli, J. M.; Yang, W.; Goodenough, J. B.; Dabrowski, B.; Freeland, J. W.; Shao-Horn, Y. Estimating hybridization of transition metal and oxygen states in perovskites from O K-edge X-ray absorption spectroscopy. *J. Phys. Chem. C* **2014,** *118*, 1856-1863.

(10) Zhou, W.; Sunarso, J. Enhancing bi-functional electrocatalytic activity of perovskite by temperature shock: A case study of $LaNiO_{3-\delta}$. *J. Phys. Chem. Lett.* **2013,** *4*, 2982-2988.

(11) Petrie, J. R.; Cooper, V. R.; Freeland, J. W.; Meyer, T. L.; Zhang, Z.; Lutterman, D. A.; Lee, H. N. Enhanced bifunctional oxygen catalysis in strained $LaNiO_3$ perovskites. *J. Am. Chem. Soc.* **2016,** *138*, 2488-2491.

(12) Li, H.; Chen, Y.; Xi, S.; Wang, J.; Sun, S.; Sun, Y.; Du, Y.; Xu, Z. J. Degree of geometric tilting determines the activity of FeO_6 octahedra for water oxidation. *Chem. Mater.* **2018,** *30*, 4313-4320.

(13) Gracia, J.; Sharpe, R.; Munarriz, J. Principles determining the activity of magnetic oxides for electron transfer reactions. *J. Catal.* **2018,** *361*, 331-338.

(14) Sharpe, R.; Munarriz, J.; Lim, T.; Jiao, Y.; Niemantsverdriet, J. W.; Polo, V.; Gracia, J. Orbital physics of perovskites for the oxygen evolution reaction. *Top. Catal.* **2018**, *61*, 267-275.

(15) Sharpe, R.; Lim, T.; Jiao, Y.; Niemantsverdriet, J. W. H.; Gracia, J. Oxygen evolution reaction on perovskite electrocatalysts with localized spins and orbital rotation symmetry. *ChemCatChem* **2016,** *8*, 3762-3768.

(16) Mefford, J. T.; Rong, X.; Abakumov, A. M.; Hardin, W. G.; Dai, S.; Kolpak, A. M.; Johnston, K. P.; Stevenson, K. J. Water electrolysis on $La_{1-x}Sr_xCoO_{3-\delta}$ perovskite electrocatalysts. *Nat. Commun.* **2016,** *7*, 11053.

(17) Suntivich, J.; May, K. J.; Gasteiger, H. A.; Goodenough, J. B.; Shao-Horn, Y. A perovskite oxide optimized for oxygen evolution catalysis from molecular orbital principles. *Science* **2011,** *334*, 1383-1385.

(18) Grimaud, A.; May, K. J.; Carlton, C. E.; Lee, Y. L.; Risch, M.; Hong, W. T.; Zhou, J.; Shao-Horn, Y. Double perovskites as a family of highly active catalysts for oxygen evolution in alkaline solution. *Nat. Commun.* **2013,** *4*, 2439.

(19) Hong, W. T.; Stoerzinger, K. A.; Lee, Y.-L.; Giordano, L.; Grimaud, A.; Johnson, A. M.; Hwang, J.; Crumlin, E. J.; Yang, W.; Shao-Horn, Y. Charge-transfer-energy-dependent oxygen evolution reaction mechanisms for perovskite oxides. *Energy Environ. Sci.* **2017,** *10*, 2190-2200.

(20) Yamada, I.; Takamatsu, A.; Asai, K.; Ohzuku, H.; Shirakawa, T.; Uchimura, T.; Kawaguchi, S.; Tsukasaki, H.; Mori, S.; Wada, K.; Ikeno, H.; Yagi, S. Synergistically enhanced oxygen evolution reaction catalysis for multielement transition-metal oxides. *ACS Appl. Energy Mater.* **2018,** *1*, 3711-3721.

(21) Toyoda, K.; Hinogami, R.; Miyata, N.; Aizawa, M. Calculated descriptors of catalytic activity for water electrolysis anode: Application to delafossite oxides. *J. Phys. Chem. C* **2015,** *119*, 6495-6501.

(22) Wei, C.; Feng, Z.; Scherer, G. G.; Barber, J.; Shao-Horn, Y.; Xu, Z. J. Cations in octahedral sites: A descriptor for oxygen electrocatalysis on transition-metal spinels. *Adv. Mater.* **2017,** *29*, 1606800.

(23) Hong, W. T.; Welsch, R. E.; Shao-Horn, Y. Descriptors of oxygen-evolution activity for oxides: A statistical evaluation. *J. Phys. Chem. C* **2016,** *120*, 78-86.

(24) Li, M.; Zhou, W.; Peterson, V. K.; Zhao, M.; Zhu, Z. A comparative study of $SrCo_{0.8}Nb_{0.2}O_{3-\delta}$ and $SrCo_{0.8}Ta_{0.2}O_{3-\delta}$ as low-temperature solid oxide fuel cell cathodes: effect of non-geometry factors on the oxygen reduction reaction. *J. Mater. Chem. A* **2015,** *3*, 24064-24070.

(25) Yagi, S.; Yamada, I.; Tsukasaki, H.; Seno, A.; Murakami, M.; Fujii, H.; Chen, H.; Umezawa, N.; Abe, H.; Nishiyama, N.; Mori, S. Covalency-reinforced oxygen evolution reaction catalyst. *Nat. Commun.* **2015,** *6*, 8249.

(26) Yamada, I.; Fujii, H.; Takamatsu, A.; Ikeno, H.; Wada, K.; Tsukasaki, H.; Kawaguchi, S.; Mori, S.; Yagi, S. Bifunctional oxygen reaction catalysis of quadruple manganese perovskites. *Adv. Mater.* **2017,** *29*, 1603004.

(27) Chamberland, B. L. Preparation and properties of $SrCrO_3$. *Solid State Commun.* **1967,** *5*, 663-666.

(28) Range, K.-J.; Rau, F.; Klement, U. High-Pressure Synthesis and Structure Refinement of $SrVO_3$, Sr_2VO_4, and $Sr_3V_2O_7$. *Z. Naturforsch. B* **1991,** *46*, 1315-1318.

(29) Kawasaki, S.; Takano, M.; Takeda, Y. Ferromagnetic properties of $SrFe_{1-x}Co_xO_3$ synthesized under high pressure. *J. Solid State Chem.* **1996,** *121*, 174-180.

(30) Belik, A. A.; Matsushita, Y.; Katsuya, Y.; Tanaka, M.; Kolodiazhnyi, T.; Isobe, M.; Takayama-Muromachi, E. Crystal structure and magnetic properties of 6*H*-$SrMnO_3$. *Phys. Rev. B* **2011,** *84*, 094438.

(31) Kawaguchi, S.; Takemoto, M.; Osaka, K.; Nishibori, E.; Moriyoshi, C.; Kubota, Y.; Kuroiwa, Y.; Sugimoto, K. High-throughput powder diffraction measurement system consisting of multiple MYTHEN detectors at beamline BL02B2 of SPring-8. *Rev. Sci. Instrum.* **2017,** *88*, 085111.

(32) Izumi, F.; Momma, K. Three-dimensional visualization in powder diffraction. *Solid State Phenom.* **2007,** *130*, 15-20.

(33) Blöchl, P. E. Projector augmented-wave method. *Phys. Rev. B* **1994,** *50*, 17953-17979.

(34) Kresse, G.; Furthmüller, J. Efficient iterative schemes for *ab initio* total-energy calculations using a plane-wave basis set. *Phys. Rev. B* **1996,** *54*, 11169-11186.

(35) Kresse, G.; Furthmüller, J. Efficiency of ab-initio total energy calculations for metals and semiconductors using a plane-wave basis set. *Comput. Mater. Sci.* **1996,** *6*, 15-50.

(36) Dudarev, S. L.; Botton, G. A.; Savrasov, S. Y.; Humphreys, C. J.; Sutton, A. P. Electron-energy-loss spectra and the structural stability of nickel oxide: An LSDA+U study. *Phys. Rev. B* **1998,** *57*, 1505-1509.

(37) Wang, Y.; Guo, G. Robust half-metallic antiferromagnets La*A*VOsO_6 and La*A*MoYO_6 (*A* = Ca, Sr, Ba; Y=Re, Tc) from first-principles calculations. *Phys. Rev. B* **2006,** *73*, 064424.

(38) Hu, Z.; Metiu, H. Choice of *U* for DFT+*U* Calculations for Titanium Oxides. *J. Phys. Chem. C* **2011,** *115*, 5841-5845.

(39) Wu, Z.; Sun, L.-P.; Xia, T.; Huo, L.-H.; Zhao, H.; Rougier, A.; Grenier, J.-C. Effect of Sr doping on the electrochemical properties of bi-functional oxygen electrode $PrBa_{1-x}Sr_xCo_2O_{5+\delta}$. *J. Power Sources* **2016,** *334*, 86-93.

(40) Sankannavar, R.; Sarkar, A. The electrocatalysis of oxygen evolution reaction on $La_{1-x}Ca_xFeO_{3-\delta}$ perovskites in alkaline solution. *Int. J. Hydrogen Energy* **2018,** *43*, 4682-4690.

(41) Cady, C. W.; Gardner, G.; Maron, Z. O.; Retuerto, M.; Go, Y. B.; Segan, S.; Greenblatt, M.; Dismukes, G. C. Tuning the Electrocatalytic water oxidation properties of AB_2O_4 spinel nanocrystals: A (Li, Mg, Zn) and B (Mn, Co) site variants of $LiMn_2O_4$. *ACS Catal.* **2015,** *5*, 3403-3410.

(42) Su, C.; Wang, W.; Chen, Y.; Yang, G.; Xu, X.; Tade, M. O.; Shao, Z. $SrCo_{0.9}Ti_{0.1}O_{3-\delta}$ As a new electrocatalyst for the oxygen evolution reaction in alkaline electrolyte with stable performance. *ACS Appl. Mater. Interfaces* **2015,** *7*, 17663-17670.

(43) Chen, C.; Baiyee, Z. M.; Ciucci, F. Unraveling the effect of La A-site substitution on oxygen ion diffusion and oxygen catalysis in perovskite $BaFeO_3$ by data-mining molecular dynamics and density functional theory. *Phys. Chem. Chem. Phys.* **2015,** *17*, 24011-24019.

(44) Guo, Y.; Tong, Y.; Chen, P.; Xu, K.; Zhao, J.; Lin, Y.; Chu, W.; Peng, Z.; Wu, C.; Xie, Y. Engineering the electronic state of a perovskite electrocatalyst for synergistically enhanced oxygen evolution reaction. *Adv. Mater.* **2015,** *27*, 5989-5994.

(45) Meng, J.; Liu, X.; Yao, C.; Zhang, X.; Liu, X.; Meng, F.; Meng, J. Investigations on structures, thermal expansion and electrochemical properties of $La_{0.75}Sr_{0.25}Cu_{0.5-x}Co_xMn_{0.5}O_{3-\delta}$ (x = 0, 0.25, and 0.5) as potential cathodes for intermediate temperature solid oxide fuel cells. *Electrochim. Acta* **2015,** *186*, 262-270.

(46) Ali, S. M.; Al-Rahman, Y. M. A. Catalytic activity of $LaBO_3$ for OER in $HClO_4$ medium: An approach to the molecular orbital theory. *J. Electrochem. Soc.* **2015,** *163*, H81-H88.

(47) Muñoz-García, A. B.; Pavone, M. K-doped $Sr_2Fe_{1.5}Mo_{0.5}O_{6-\delta}$ predicted as a bifunctional catalyst for air electrodes in proton-conducting solid oxide electrochemical cells. *J. Mater. Chem. A* **2017,** *5*, 12735-12739.

(48) Pramana, S. S.; Cavallaro, A.; Li, C.; Handoko, A. D.; Chan, K. W.; Walker, R. J.; Regoutz, A.; Herrin, J. S.; Yeo, B. S.; Payne, D. J.; Kilner, J. A.; Ryan, M. P.; Skinner, S. J. Crystal structure and surface characteristics of Sr-doped $GdBaCo_2O_{6-\delta}$ double perovskites: oxygen evolution reaction and conductivity. *J. Mater. Chem. A* **2018,** *6*, 5335-5345.

Table of Contents Graphic